Manipulating a Whip in 3D via Dynamic Primitives*

Moses C. Nah[1], Aleksei Krotov[2], Marta Russo[3,4], Dagmar Sternad[4,5] and Neville Hogan[1,6]

***Abstract*— A prominent challenge in the field of robotics is manipulation of flexible objects. One major factor that makes this task difficult is the complex dynamics emerging from its high-dimensional structure. This argues against the use of popular optimization-based approaches, which scale poorly with system dimension (the "curse of dimensionality"). Nevertheless, almost indifferent to this complexity, humans handle it on a daily basis, without any apparent difficulty.**

Inspired by human motor control, we propose that encoding movements based on dynamic primitives can simplify the task of manipulating flexible objects and provides a way around the curse of dimensionality. Using an extreme example — manipulating a whip — we tested in simulation whether targets at various locations could be reached with a whip by using a controller based on dynamic primitives. Regardless of the target location, this approach successfully managed the complexity of a 54 degree-of-freedom system (yielding a 108-dimensional state-space representation) and identified an upper-limb movement that achieved the task. This approach did not require a detailed model of the whip, which thereby significantly simplified the computational complexity of the control task. We believe that this approach may facilitate robotic manipulation of flexible materials, and in general afford a simplified way to control dynamically complex objects.

I. Introduction

Endowing robots with human-level dexterity is one of the ultimate goals of robotics. While the gap between human and robot performance is rapidly closing, humans' astonishing dexterity is still far superior to anything yet achieved in robotic systems [1].

The disparity in performance becomes more evident when the task involves manipulation of flexible objects with significant dynamics. The complex dynamics emerging from their high degrees of freedom (DOF) structure is one of the many factors which makes this task challenging. Due to the high-dimensional structure, popular optimization-based approaches, which scale poorly with system dimension, often fail to identify the optimal solution (the notorious "curse of dimensionality") [2]. Nevertheless, humans are strikingly adept at manipulating flexible objects, without any apparent difficulty. With care, understanding the strategy which humans use to handle flexible objects may allow us to better bridge the gap between humans and robots.

Mounting evidence suggests that humans compose actions based on dynamic primitives to simplify control [3]–[7]. Dynamic primitives are conceived as "dynamic attractors" which act as fundamental building blocks of motor behavior [8]–[10]. At least three distinct classes of dynamic primitives have been identified — submovements, oscillations and mechanical impedances. We propose that encoding actions based on dynamic primitives could facilitate robotic control of flexible, deformable objects.

To test this proposition, we focused on a task of striking a distant target with a whip — one of the most complex and exotic tools which humans can handle [11]. Extending the work reported in [12] in which the arm, whip and target were confined to a 2D sagittal plane, the work reported here generalized the case to 3D. We considered spatial motions of human upper limb and whip, and several different target locations in 3D space. We formulated and parameterized a 4-DOF model of the human arm interacting with a 50-DOF whip model, for which the model parameters were derived from an actual bullwhip [12], [13]. We used a feedforward motion command composed of a single submovement planned in joint-space coordinates and constant mechanical impedances for the upper-limb controller.

We discovered that regardless of the target location, this approach was able to manage the complexity of a 54-DOF system (yielding a 108-dimensional state-space representation) and succeeded to identify an upper-limb movement that achieved the task. Encoding movements with parameterized dynamic primitives significantly simplified the task of placing the tip of the whip at arbitrary locations and offered a way to work around the curse of dimensionality. This result demonstrated the effectiveness of dynamic primitives to control an extremely high-DOF object. We believe that this approach will facilitate robotic manipulation of flexible objects, which is currently a major challenge.

II. Methods

The research presented in this paper used the simulation software MuJoCo [14]. For all of the MuJoCo simulations, the semi-implicit Euler method was chosen as the numerical integrator, with a time step of 0.1ms (10,000Hz).

A. Modelling

The model used in the MuJoCo simulation consisted of two main parts: a model of a human upper limb (the manip-

*Supported in part by NSF M3X-1826097 (Neville Hogan) and NSF M3X-1825942 (Dagmar Sternad), and NIH-R01-HD087089.

[1]Department of Mechanical Engineering, Massachusetts Institute of Technology, Cambridge, MA, USA

[2]Department of Bioengineering, Northeastern University, Boston, MA, USA. Supported in part by Fulbright-IIE-PS00261102

[3]Department of Neurology, Policlinico Tor Vergata and the Laboratory of Neuromotor Physiology, IRCCS Santa Lucia Foundation, Rome, Italy.

[4]Department of Biology, Northeastern University, Boston, MA, USA

[5]Department of Electrical and Computer Engineering, Department of Physics, Institute for Experiential Robotics, Northeastern University, Boston, MA, USA

[6]Department of Brain and Cognitive Sciences, Massachusetts Institute of Technology, Cambridge, MA, USA

Email addresses: mosesnah@mit.edu, krotov.a@northeastern.edu, marta.russo.phd@gmail.com, d.sternad@northeastern.edu, neville@mit.edu

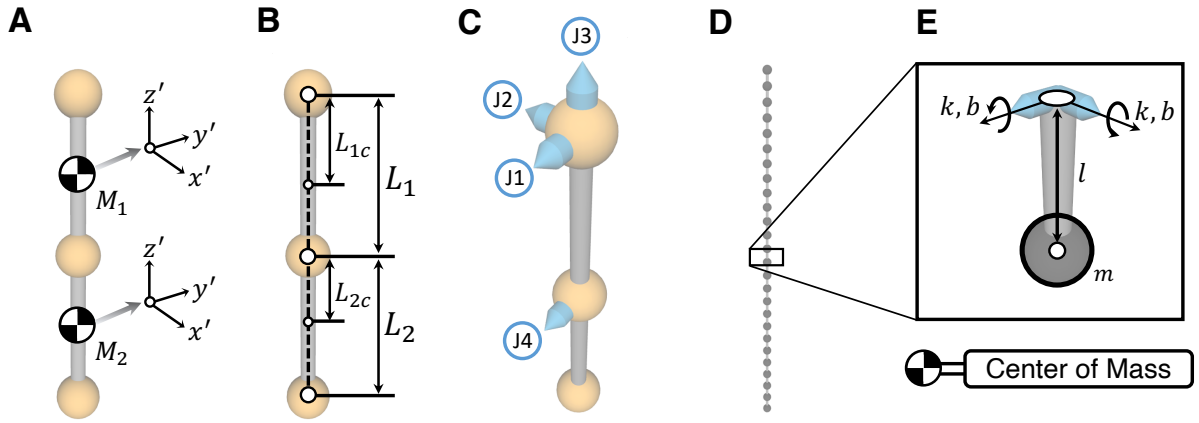

Fig. 1: The upper-limb (**A**-**C**) and whip model (**D**-**E**) rendered with the MuJoCo simulator. (**A**) Mass, principal axes of inertia and the reference frame of each limb segment (Table I). (**B**) Length of each limb segment and length from proximal joint to center of mass (COM) (Table I). (**C**) Rotational joints of shoulder (J1 J3) and elbow (J4) and their axes of rotation. (**D**) The 50-DOF whip model. (**E**) Length l and mass m of the sub-model of the whip, rotational joints which serially connect the sub-models, and their axes of rotation. Each rotational joint was equipped with a linear rotational spring k and rotational damper b. Axes of rotation are visualized as bullet shapes.

ulator) and a model of a whip (the object being manipulated).

1) 4-DOF Upper-limb Model: The human arm was modeled as a two-bar open-chain linkage. Everything distal to the wrist (i.e., hand, fingers etc.) were omitted from this model. The two limb segments — the upper arm (which extends from the shoulder to the elbow), and the forearm (which extends from the elbow to the wrist) — were treated as non-uniform cylinders, i.e., the center of mass (COM) did not coincide with the geometric center of the limb segment. The geometrical and inertial parameters of each limb segment were obtained from a computational model by Hatze [15], and the detailed values are presented in Table I (Fig. 1, 2).

The upper-limb model had 4-DOF — 3-DOF at the shoulder and 1-DOF at the elbow. The ball-socket mechanism of the shoulder's glenohumeral joint was modeled as a 3-DOF spherical joint. Translation movements of the shoulder were omitted from the model, i.e., the shoulder joint was fixed in space. The 3-DOF spherical joint was constructed as a sequence of three rotational joints whose axes of rotation were initially orthogonal — denoted as J1-J3 (Fig. 1C). The three rotational joints in order, corresponded to flexion/extension (J1), adduction/abduction (J2) and lateral/medial rotation (J3). The movement of the elbow was modeled as single-joint elbow flexion/extension (J4) (Fig. 1C). Supination/pronation of the elbow was omitted from the model. At all four joints, independently controlled torque actuators were mounted.

2) 50-DOF Whip Model: The continuous structure of a whip was approximated and discretized as a multi-link pendulum composed of (ideal) lumped elements. Each sub-model (i.e., pendulum) of the whip consisted of three lumped-parameter elements: an (ideal) point-mass, a linear rotational spring and a linear rotational damper (Fig. 1D, 1E). The point-mass m was suspended from a massless cylinder with length l. The other end of the massless cylinder was equipped with a 2-DOF universal joint, which consisted of two rotational joints whose axes of rotation were orthogonal. Each rotational joint was equipped with a linear rotational spring and a linear rotational damper, with coefficients k and b, respectively (Fig. 1E). The values of the model parameters of the whip were obtained from an "experimentally-fitted" whip model, in which the values were derived from experimental observations of an actual bullwhip [12], [13]. 25 of the identical 2-DOF sub-models were serially connected, which resulted in a 50-DOF whip model.

3) Connection between the Two Models: To not introduce any additional torque between the upper-limb and the whip model, the rotational stiffness k and damping coefficient b of the whip sub-model, which directly attached to the end-effector of the upper-limb model, were set as zero. Summarizing, the whole system resulted in a 54-DOF open-chain linkage.

B. Controller

1) Impedance Controller: A first-order impedance controller with gravity compensation was used for the upper-limb controller [16]:

$$\boldsymbol{\tau} = \boldsymbol{K}\left(\boldsymbol{\phi} - \boldsymbol{\theta}\right) + \boldsymbol{B}\left(\dot{\boldsymbol{\phi}} - \dot{\boldsymbol{\theta}}\right) + \boldsymbol{\tau}_G \tag{1}$$

where $\boldsymbol{K}, \boldsymbol{B} \in \mathbb{R}^{4\times4}$ are constant joint stiffness and damping matrices, which account for the neuromuscular mechanical impedance of the upper-limb model; $\boldsymbol{\tau} \in \mathbb{R}^4$ denotes the net-torque input of each joint actuator; $\boldsymbol{\theta} \in \mathbb{R}^4$ denotes the actual joint displacements of the upper-limb model; $\boldsymbol{\phi} \in \mathbb{R}^4$ denotes the "zero-torque" trajectory, i.e., neglecting gravitational effects, no torque will be exerted by the actuator when $\boldsymbol{\phi}$ exactly matches the actual joint displacements $\boldsymbol{\theta}$ [12]; $\boldsymbol{\tau}_G \in \mathbb{R}^4$ denotes the torque required to compensate the gravitational forces applied to the whole system (Sec. II-B.2). The zero-torque trajectory $\boldsymbol{\phi}(t)$ was the feedforward motion command of the controller which generated the upper-limb movement (Sec. II-B.3).

TABLE I: The Model Parameters

	Description	Notation	Values	Units
Limb Inertia Parameters	Mass of each limb segment	M_1 , M_2	1.595 , 0.869	[kg]
	Length of each limb segment	L_1 , L_2	0.294 , 0.291	[m]
	Length from proximal joint to COM	L_{1c} , L_{2c}	0.129 , 0.112	[m]
	Principal moment of inertia, x'-axis	$I_{1,xx}$, $I_{2,xx}$	0.0119, 0.0048	[kg·m^2]
	Principal moment of inertia, y'-axis	$I_{1,yy}$, $I_{2,yy}$	0.0119, 0.0049	[kg·m^2]
	Principal moment of inertia, z'-axis	$I_{1,zz}$, $I_{2,zz}$	0.0013, 0.0005	[kg·m^2]
Parameters of the Whip Model	Number of sub-models	N	25	[-]
	Value of the point-mass	m	0.012	[kg]
	Length of massless cylinder	l	0.072	[m]
	Coefficient of the rotational spring	k	0.242	[N·m/rad]
	Coefficient of the rotational damper	b	0.092	[N·m·s/rad]

(Top) The geometrical and inertial parameters of the upper-limb model. Subscripts denote the shoulder and elbow joints, numbered proximal to distal. Principal moments of inertia of limb segments were calculated with respect to the center of mass (COM) (Fig. 1A, 1B, 1C). (Bottom) The parameters of the whip model, which were measured and experimentally derived from an actual bullwhip. Graphical depictions of the upper-limb and whip models are shown in (Fig. 1, 2)

2) Gravity Compensation: Gravitational effects were compensated with $\boldsymbol{\tau}_G$, so that the actual upper-limb posture $\boldsymbol{\theta}$ could exactly match the zero-torque posture $\boldsymbol{\phi}$ when the whole model was at rest:

$$\boldsymbol{\tau}_G = \boldsymbol{J}_{01}^T \boldsymbol{f}_{1,G} + \boldsymbol{J}_{02}^T \boldsymbol{f}_{2,G} + \boldsymbol{J}_{03}^T \boldsymbol{f}_{3,G} \tag{2}$$

where $\boldsymbol{J}_{ij} \in \mathbb{R}^{3\times4}$ is a Jacobian matrix of frame j relative to frame i; $\boldsymbol{f}_{i,G} \in \mathbb{R}^3$ denotes the gravitational force applied to frame i; frame 0, 1, 2 and 3 are attached to the shoulder, COM of the upper arm, COM of the forearm, and the end-effector of the upper-limb model (Fig. 2).

The detailed force vectors are as follows:

$$\boldsymbol{f}_{1,G} = M_1\boldsymbol{g}, \quad \boldsymbol{f}_{2,G} = M_2\boldsymbol{g}, \quad \boldsymbol{f}_{3,G} = M_w\boldsymbol{g} \tag{3}$$

where M_1 and M_2 denote the mass of upper arm and forearm, respectively (Table I); M_w denotes the total mass of the whip model, which is the number of sub-models of the whip N multiplied by the point-mass m ($M_w = N \cdot m =$ 0.3kg); $\boldsymbol{g} \in \mathbb{R}^3$ denotes the gravity vector (Fig. 2).

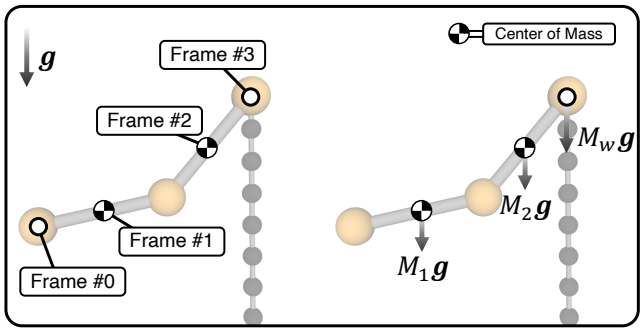

Fig. 2: Frames and the imposed gravitational forces of the simulation model.

3) Motion Planning – Zero-Torque Trajectory: The zero-torque trajectory $\boldsymbol{\phi}(t)$ (Eq. 1) of the upper-limb model consisted of a single movement — a discrete minimum-jerk profile planned in joint coordinates [17] (Sec. IV-B).

$$\boldsymbol{\phi}(t) = \boldsymbol{\phi}_i + (\boldsymbol{\phi}_f - \boldsymbol{\phi}_i) \cdot \left\{ 10\left(\frac{t}{D}\right)^3 - 15\left(\frac{t}{D}\right)^4 + 6\left(\frac{t}{D}\right)^5 \right\} \tag{4}$$

where subscripts i and f denote the initial and final (zero-torque) postures, respectively; D denotes the duration of the movement. For times greater than duration D (i.e., $t > D$), the zero-torque trajectory of the upper-limb model remained at final posture $\boldsymbol{\phi}_f$. The zero-torque trajectory $\boldsymbol{\phi}(t)$ was determined by 9 movement parameters: 4 for initial posture $\boldsymbol{\phi}_i$, 4 for final posture $\boldsymbol{\phi}_f$, and 1 for movement duration D.

4) Stiffness and Damping Matrices: The neuromuscular mechanical impedance $\boldsymbol{K}$ and $\boldsymbol{B}$ matrices (Eq. 1) were chosen to be symmetric positive-definite matrices. The damping matrix $\boldsymbol{B}$ was chosen to be proportional to joint stiffness $\boldsymbol{K}$ such that $\boldsymbol{B} = \beta\boldsymbol{K}$ for a positive constant $\beta = 0.05$s. The detailed values used for the stiffness matrix $\boldsymbol{K}$ and damping matrix $\boldsymbol{B}$ were as follows (Sec. IV-C):

$$\boldsymbol{K} = \begin{bmatrix} 17.4 & 6.85 & -7.75 & 8.40 \\ 6.85 & 33.0 & 3.70 & 0.00 \\ -7.75 & 3.70 & 27.7 & 0.00 \\ 8.40 & 0.00 & 0.00 & 23.2 \end{bmatrix}, \quad \boldsymbol{B} = 0.05\boldsymbol{K} \tag{5}$$

C. Task Definition and Optimization

A whip task was defined to evaluate the performance of the upper-limb controller. The goal of the task was to hit a distant target with the tip of the whip. Quantitatively, the objective was to minimize the value L [m], the distance between the tip of the whip and target with a single discrete upper-limb movement, i.e., a single set of 9 movement parameters of the zero-torque trajectory $(\boldsymbol{\phi}_i, \boldsymbol{\phi}_f, D)$ (Eq. 4). The minimum value of the distance L reached with a single discrete upper-limb movement, L^* [m] was a quantitative measure to assess movement performance.

Three different target locations were defined for the whip task. All three targets were distanced just 0.01m outside of a sphere, centered at the shoulder joint, of radius R [m]

equal to the sum of the lengths of the upper-limb and whip model ($R = L_1 + L_2 + N \cdot l + 0.01 = 2.395$m) (Table I). This offset avoided the whip model colliding with a target, which prevented unnecessary contact dynamics being included in the simulation, while retaining the qualitative and quantitative goal of the whip task. In a spherical coordinate system (radius-azimuth-elevation), target 1, 2 and 3 were located at coordinate $(R, 0°, 0°)$, $(R, 45°, 0°)$ and $(R, 45°, 45°)$, respectively (Fig. 3).

For each target location, the optimal 9 movement parameters (ϕ_i, ϕ_f, D) which minimized the minimum distance between the tip of the whip and target, were identified with a global derivative-free optimization algorithm DIRECT-L (DIviding RECTangles Locally biased) under the nlopt (nonlinear optimization) Python tool box [18]. Within the bounds of the constraint (Table II), the DIRECT-L optimization algorithm conducted 600 iterations.

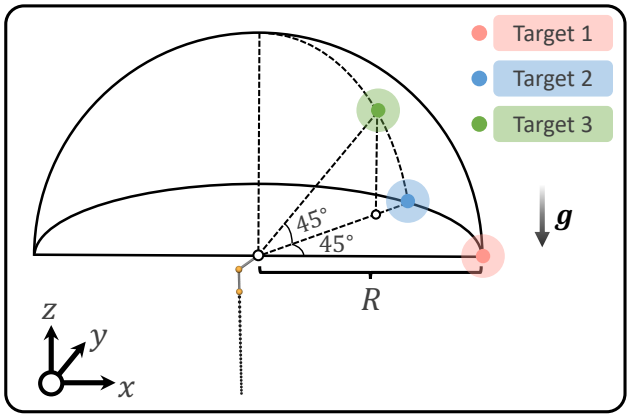

Fig. 3: Graphical depiction of the three target positions of the targeting task, and the coordinate frame of the simulation.

III. Optimization Results

For each target location, the DIRECT-L algorithm converged to an optimal set of 9 movement parameters which resulted in a minimum value of distance L^*. Detailed values of the optimal parameters of the movement and its corresponding L^* value are presented in Table II. Three timeframes of the simulation results generated by the optimal movement parameters, visualized using MATLAB (Mathworks Inc., Natick, MA), are shown in Fig. 4.

IV. Discussion

A. Simplification of the Whip Task

This study examined in simulation whether a target at various locations in 3D space could be reached with a whip using a (small) number of primitive actions, whose parameters could be learned through optimization. Considering the dimensionality of the whole system, this task is by no means trivial — the task was to coordinate a system with 108 state-space dimensions in 3D space to reach targets at several locations. Despite this daunting complexity, encoding upper-limb action using the parameters of a single movement dramatically simplified the targeting task and successfully managed the complexity of an extremely high-dimensional system. This approach provided a way to work around the curse of dimensionality and the algorithm was able to converge to an optimal upper-limb movement.

It is worth emphasizing that this method completely avoided the need to acquire a detailed and accurate model of the whip. Regardless of the dimensionality or complexity of the object dynamics, the manipulation task was substituted by the optimization of a small set of movement parameters. This approach seems to be a key simplification required to learn complex motor skills, since only a small set of parameters are acquired and retained regardless of the complexity of the object. Moreover, assuming the existence of a well-defined objective function, we believe that this method can be generalized and may afford a simplified way to control dynamically complex objects.

B. Simplified Motion Planning via Dynamic Primitives

While tremendous progress has been achieved in the manipulation of rigid objects, flexible object manipulation remains to be a long-standing problem. One of the significant challenges is motion planning for flexible object manipulation, since the complex dynamics of the object leads to unpredictable behavior [19], [20]. To tackle this problem, studies depended on human demonstrators, required an extremely large set of data to learn the task, or often involved vision algorithms to detect key features, along with an analytical model of the object [21], [22]. However, these methods still suffer from the complexity emerging from the high-dimensional structure of the object.

The approach presented in this paper does not rely on any specific analytical model nor visual observation of the whip. By composing movements based on dynamic primitives, the method reported here succeeded to manipulate a flexible object with significant dynamics, without the need to acquire or extract any data from human demonstrations, and with a modest number of iterations of the optimization. Planning a feedforward open-loop motion command $\boldsymbol{\phi}(t)$ (Eq. 4), with constant impedance terms $\boldsymbol{K}$ and $\boldsymbol{B}$, was sufficient to manipulate a 50-DOF whip model for the targeting task.

Previous study suggests that for tasks involving complex interaction dynamics, the minimum-jerk principle has limited value [23]. This fact was demonstrated in a task of transporting a nonlinear cup-and-ball system, which was not competently achieved with a single minimum-jerk profile. The result presented in this paper provides an intriguing counter-example — the targeting task involved an interaction with a 50-DOF model and a minimum-jerk (nominal) motion was still able to manage this complexity. The dimensionality of the object (50-DOF vs. 2-DOF) may account for this difference, although further clarification remains to be established.

Although the method presented in this paper provided an effective way to reduce the dimensionality of the optimization problem, we want to emphasize that this result does not preclude alternative approaches. For example, an input time-history (e.g., of joint torques) might be defined by a

TABLE II: The Upper, Lower Bound of the Search Space, Optimal Movement Parameters

		Movement Parameters									
		$\phi_{1,i}$ [rad]	$\phi_{2,i}$ [rad]	$\phi_{3,i}$ [rad]	$\phi_{4,i}$ [rad]	$\phi_{1,f}$ [rad]	$\phi_{2,f}$ [rad]	$\phi_{3,f}$ [rad]	$\phi_{4,f}$ [rad]	D [s]	L^* [m]
Bounding Box Constraints	Lower Bound	-0.5π	-0.5π	-0.5π	0.0π	0.1π	-0.5π	-0.5π	0.0π	0.4	
	Upper Bound	-0.1π	0.5π	0.5π	0.9π	1.0π	0.5π	0.5π	0.9π	1.5	
Optimal Movement Parameters	Target 1	−1.501	0.000	−0.237	1.414	1.728	0.000	0.000	0.332	0.950	0.051
	Target 2	−1.103	0.737	−0.233	2.310	1.728	−1.034	−1.396	0.192	0.579	0.092
	Target 3	−0.943	0.815	−1.396	1.728	2.670	−0.698	−1.396	0.052	0.950	0.127

sparse number of knot points connected by some suitable spline function, and that may also facilitate convergence of the optimization. In essence, the discrete motion profile used here is an extreme example of that approach, using only two knot points in the $\mathbb{R}^4$ space for the entire trajectory. One should note, however, that the choice of motion profile was not arbitrary, but based on biological observation of human movements in multiple situations [17], [24].

C. Justification of the Stiffness and Damping Matrices

Three key modelling assumptions were used to determine the $\boldsymbol{K}$ and $\boldsymbol{B}$ matrices (Eq. 5):

- *The neuromuscular stiffness corresponding to shoulder joints J2, J3 (excluding the shoulder flexion/extension joint, J1) and elbow joint J4 were perfectly decoupled.*
  — Intrinsic neuromechanical impedance arises from the properties of muscles and their activation. Several multi-articular muscles exist which couple motion across the shoulder and elbow joints [25]. Hence, multi-articular muscles result in off-diagonal stiffness terms between the shoulder and elbow joint. For simplicity, we assumed that the coupling between joint J1 and J4 was largely predominant, such that the cross-coupling stiffness terms between shoulder joint J2, J3 and elbow joint J4 could be neglected.
- *The stiffness matrix $\boldsymbol{K}$ was chosen to be symmetric.*
  — Studies have shown that the force field emerging from the elastic properties of the upper limb musculature is nearly curl-free, meaning that the stiffness matrix of the neuromuscular impedance of the upper extremity is predominantly symmetric [26]. In principle, symmetry of the stiffness matrix is consistent with passivity (i.e., the system may store energy and release it, but cannot continuously supply power), which plays a key role in preventing instability due to physical contact and dynamic interaction with passive objects [27].
- *The damping matrix $\boldsymbol{B}$ was chosen to be proportional to joint stiffness $\boldsymbol{K}$, i.e., $\boldsymbol{B} = \beta \boldsymbol{K}$ for some constant β.*
  — To model the dynamics of the first-order impedance controller with a single time-constant, values for the joint damping matrix $\boldsymbol{B}$ were assumed to be proportional to the joint stiffness matrix $\boldsymbol{K}$. For this upper-limb controller, the time-constant β was set as 0.05s [28] (Eq. 5).

Along with these key assumptions, experimental measurements [29], [30] were used to construct the stiffness matrix $\boldsymbol{K}$ and damping matrix $\boldsymbol{B}$ of the upper-limb controller, which resulted in a motion resembling the actual motor behavior of the upper limb.

D. Relation to Prior Work

Composing a controller based on dynamic primitives offered a simplified solution for complex object manipulation. A single movement planned in joint-space coordinates, which corresponds to a motion primitive, and constant impedance terms described by $\boldsymbol{K}$ and $\boldsymbol{B}$ which account for physical interactions, were able to manage the complex dynamics of the whip [8]–[10].

Note that the idea of simplifying motor control via primitive elements is not at all new. Approaches using dynamic movement primitives have been proposed as a powerful, robust and adaptive method for various tasks [4], [31]–[33]. Nevertheless, to the best of our knowledge, this prior work mainly focused on unconstrained movements or on the manipulation of rigid objects with comparatively low system dimensions. Tasks which involve objects as dynamically complex as a whip have not been fully explored. The study presented in this paper has expanded the feasibility of primitives-based approaches by managing a very complex object using just one motion primitive.

As used in the work reported here, dynamic primitives include mechanical impedances to account for physical interaction with the object [8]–[10]. Adding mechanical impedance as a class of dynamic primitives may facilitate the control of physical interactions [34]. However, by choosing constant impedance terms, this study did not explore the effect of different and potentially varying mechanical impedance for complex object manipulation. Studying the role of mechanical impedance is a topic of future research.

V. Conclusion

The simulations presented in this paper demonstrated that encoding control based on dynamic primitives enabled optimization to successfully identify an optimal movement that handled an extremely complex object — a whip. We anticipate that incorporating dynamic primitives to robot control systems will facilitate robotic manipulation of flexible, deformable objects, which continues to be a significant challenge.

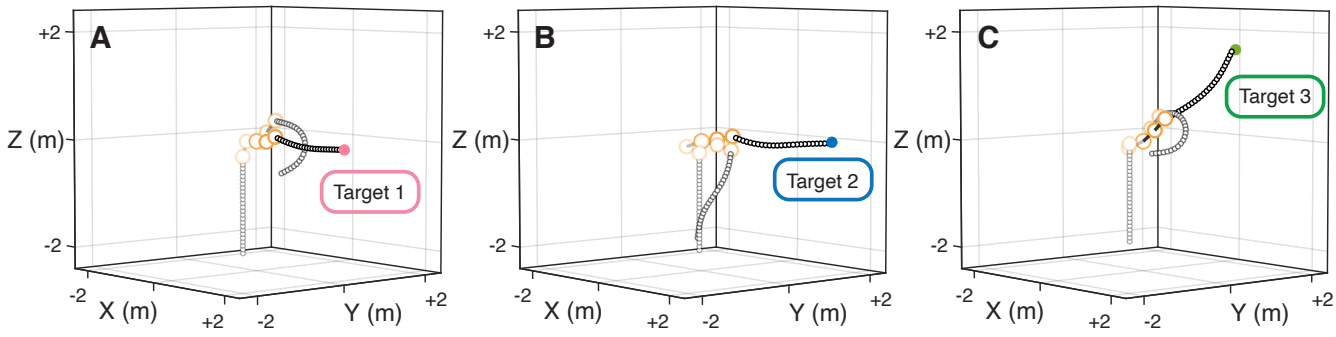

Fig. 4: The time-sequence of upper-limb (orange) and whip model (black). (**A**) Target 1 (**B**) Target 2 (**C**) Target 3. The simulation was generated by the optimal upper-limb movement parameters (Table I) and re-visualized in MATLAB. Opacity of the color increases from start to end of the movement.

REFERENCES

[1] A. Billard and D. Kragic, "Trends and challenges in robot manipulation," *Science*, vol. 364, no. 6446, 2019.

[2] R. Bellman, "Dynamic programming and stochastic control processes," *Information and Control*, vol. 1, no. 3, pp. 228–239, 1958.

[3] A. de Rugy and D. Sternad, "Interaction between discrete and rhythmic movements: reaction time and phase of discrete movement initiation during oscillatory movements," *Brain Research*, vol. 994, no. 2, pp. 160–174, 2003.

[4] R. Ronsse, D. Sternad, and P. Lefevre, "A computational model for rhythmic and discrete movements in uni-and bimanual coordination," *Neural Computation*, vol. 21, no. 5, pp. 1335–1370, 2009.

[5] D. Sternad, H. Marino, S. Charles, M. Duarte, L. Dipietro, and N. Hogan, "Transitions between discrete and rhythmic primitives in a unimanual task," *Frontiers in Computational Neuroscience*, vol. 7, p. 90, 2013.

[6] S.-W. Park, H. Marino, S. K. Charles, D. Sternad, and N. Hogan, "Moving slowly is hard for humans: limitations of dynamic primitives," *Journal of Neurophysiology*, vol. 118, no. 1, pp. 69–83, 2017.

[7] H. Guang, S. Bazzi, D. Sternad, and N. Hogan, "Dynamic primitives in human manipulation of non-rigid objects," in *International Conference on Robotics and Automation (ICRA)*, pp. 3783–3789, IEEE, 2019.

[8] N. Hogan and D. Sternad, "Dynamic primitives of motor behavior," *Biological Cybernetics*, vol. 106, no. 11-12, pp. 727–739, 2012.

[9] N. Hogan and D. Sternad, "Dynamic primitives in the control of locomotion," *Frontiers in Computational Neuroscience*, vol. 7, p. 71, 2013.

[10] N. Hogan, "Physical interaction via dynamic primitives," in *Geometric and Numerical Foundations of Movements*, pp. 269–299, Springer, 2017.

[11] A. Goriely and T. McMillen, "Shape of a cracking whip," *Physical Review Letters*, vol. 88, no. 24, p. 244301, 2002.

[12] M. C. Nah, A. Krotov, M. Russo, D. Sternad, and N. Hogan, "Dynamic primitives facilitate manipulating a whip," in *8th IEEE RAS/EMBS International Conference for Biomedical Robotics and Biomechatronics (BioRob)*, pp. 685–691, IEEE, 2020.

[13] A. D. Krotov, "Human control of a flexible object: Hitting a target with a bull-whip," Master's thesis, Northeastern University, 2020.

[14] E. Todorov, T. Erez, and Y. Tassa, "Mujoco: A physics engine for model-based control," in *IEEE/RSJ International Conference on Intelligent Robots and Systems*, pp. 5026–5033, IEEE, 2012.

[15] H. Hatze, "A mathematical model for the computational determination of parameter values of anthropomorphic segments," *Journal of Biomechanics*, vol. 13, no. 10, pp. 833–843, 1980.

[16] N. Hogan, "Impedance control: An approach to manipulation," in *American Control Conference*, pp. 304–313, 1984.

[17] T. Flash and N. Hogan, "The coordination of arm movements: an experimentally confirmed mathematical model," *Journal of Neuroscience*, vol. 5, no. 7, pp. 1688–1703, 1985.

[18] J. M. Gablonsky and C. T. Kelley, "A locally-biased form of the DIRECT algorithm," *Journal of Global Optimization*, vol. 21, no. 1, pp. 27–37, 2001.

[19] B. Nasseroleslami, C. J. Hasson, and D. Sternad, "Rhythmic manipulation of objects with complex dynamics: predictability over chaos," *PLoS Computational Biology*, vol. 10, no. 10, p. e1003900, 2014.

[20] J. Sanchez, J.-A. Corrales, B.-C. Bouzgarrou, and Y. Mezouar, "Robotic manipulation and sensing of deformable objects in domestic and industrial applications: a survey," *The International Journal of Robotics Research*, vol. 37, no. 7, pp. 688–716, 2018.

[21] Y. Yamakawa, K. Odani, and M. Ishikawa, "Sonic-speed manipulation of a bull whip using a robot manipulator," in *2016 IEEE International Conference on Advanced Intelligent Mechatronics (AIM)*, pp. 1139–1144, IEEE, 2016.

[22] A. Nair, D. Chen, P. Agrawal, P. Isola, P. Abbeel, J. Malik, and S. Levine, "Combining self-supervised learning and imitation for vision-based rope manipulation," in *IEEE International Conference on Robotics and Automation (ICRA)*, pp. 2146–2153, IEEE, 2017.

[23] S. Bazzi and D. Sternad, "Human control of complex objects: towards more dexterous robots," *Advanced Robotics*, vol. 34, no. 17, pp. 1137–1155, 2020.

[24] P. Morasso, "Spatial control of arm movements," *Experimental Brain Research*, vol. 42, no. 2, pp. 223–227, 1981.

[25] N. Hogan, "Force control with a muscle-activated endoskeleton," in *Advances in Robot Control*, pp. 201–216, Springer, 2006.

[26] F. A. Mussa-Ivaldi, N. Hogan, and E. Bizzi, "Neural, mechanical, and geometric factors subserving arm posture in humans," *Journal of Neuroscience*, vol. 5, no. 10, pp. 2732–2743, 1985.

[27] N. Hogan, "On the stability of manipulators performing contact tasks," *IEEE Journal on Robotics and Automation*, vol. 4, no. 6, pp. 677–686, 1988.

[28] J. Hermus, J. Doeringer, D. Sternad, and N. Hogan, "Separating neural influences from peripheral mechanics: the speed-curvature relation in mechanically constrained actions," *Journal of Neurophysiology*, vol. 123, no. 5, pp. 1870–1885, 2020.

[29] T. Flash, "The control of hand equilibrium trajectories in multi-joint arm movements," *Biological Cybernetics*, vol. 57, no. 4-5, pp. 257–274, 1987.

[30] D. B. Lipps, E. M. Baillargeon, D. Ludvig, and E. J. Perreault, "Quantifying the multidimensional impedance of the shoulder during volitional contractions," *Annals of Biomedical Engineering*, pp. 1–16, 2020.

[31] S. Schaal, J. Peters, J. Nakanishi, and A. Ijspeert, "Control, planning, learning, and imitation with dynamic movement primitives," in *Workshop on Bilateral Paradigms on Humans and Humanoids: IEEE International Conference on Intelligent Robots and Systems (IROS)*, pp. 1–21, 2003.

[32] J. Nakanishi, J. Morimoto, G. Endo, G. Cheng, S. Schaal, and M. Kawato, "Learning from demonstration and adaptation of biped locomotion," *Robotics and Autonomous Systems*, vol. 47, no. 2-3, pp. 79–91, 2004.

[33] S. Schaal, "Dynamic movement primitives-a framework for motor control in humans and humanoid robotics," in *Adaptive Motion of Animals and Machines*, pp. 261–280, Springer, 2006.

[34] R. Sharif Razavian, S. Bazzi, R. Nayeem, M. Sadeghi, and D. Sternad, "Dynamic primitives and optimal feedback control for the manipulation of complex objects.," in *IEEE International Conference on Robotics and Automation (ICRA)*, 2021.